galaxies

MDPI

Article

Singularities in Static Spherically Symmetric Configurations of General Relativity with Strongly Nonlinear Scalar Fields

Oleksandr Stashko * and Valery I. Zhdanov *

Astronomical Observatory, Taras Shevchenko National University of Kyiv, UA-01033 Kyiv, Ukraine; alexander.stashko@gmail.com (O.S.); valery.zhdanov@knu.ua (V.I.Z.)

Abstract: There are a number of publications on relativistic objects dealing either with black holes or naked singularities in the center. Here we show that there exist static spherically symmetric solutions of Einstein equations with a strongly nonlinear scalar field, which allow the appearance of singularities of a new type ("spherical singularities") outside the center of curvature coordinates. As the example, we consider a scalar field potential $\sim\sinh(\phi^{2n})$, $n > 2$, which grows rapidly for large field values. The space-time is assumed to be asymptotically flat. We fulfill a numerical investigation of solutions with different n for different parameters, which define asymptotic properties at spatial infinity. Depending on the configuration parameters, we show that the distribution of the stable circular orbits of test bodies around the configuration is either similar to that in the case of the Schwarzschild solution (thus mimicking an ordinary black hole), or it contains additional rings of unstable orbits.

Keywords: singularities; scalar field; circular orbits; accretion disks

Citation: Stashko, O.; Zhdanov, V.I. Singularities in Static Spherically Symmetric Configurations of General Relativity with Strongly Nonlinear Scalar Fields. *Galaxies* **2021**, *9*, 72. https://doi.org/10.3390/galaxies9040072

Academic Editor: Lorenzo Iorio

Received: 31 August 2021
Accepted: 27 September 2021
Published: 1 October 2021

1. Introduction

Nowadays, the concept of a black hole has become a common element of astrophysical research [1–3]. However, in order to be fully confident in the theoretical idea, it must be compared with alternative models. This is one of the motivations for many theoretical works devoted to non-canonical and even exotic solutions of General Relativity and its modifications, which could have similar astrophysical consequences. The non-exhaustive list below includes papers on various aspects of compact objects with naked singularities [4–14], with wormholes [15–19], boson stars [20–24], and the other non-singular objects mimicking the black holes [25–27]. The question arises as to how the aforementioned exotic configurations were formed; probably, not all corresponding models can reflect real astrophysical situations. However, final answers about the reality of these models must be based on observations. This explains why the interest in the "black hole mimickers" greatly increased after the Event Horizon Telescope observed the image of the accretion disk around the supermassive black hole in the center of M87 [28]. Correspondingly, much attention is paid to the observational manifestations of different models dealing with motion of test particles and photons in the gravitational field of the compact object [4,6,25,26,29,30]; an important point concerns the images of accretion disks, radiation fluxes, forms of the relativistic Fe $K\alpha$ line [27,31–40], etc.

A number of models are based on static solutions of the Einstein equations with scalar field (SF) [29–33,36,41]. These papers use analytically defined metrics, in particular the Fisher–Yanis–Newman–Winicour solution [42–45]. Papers [29–33,36] deal with singularities in the center, the solutions used do not have other "physical" singularities outside the center. It was proved [46] that this is a fairly general situation, at least when considering an isolated spherically symmetric configuration of General Relativity with a scalar field. Here the gravitational field suppresses the appearance of "spherical singularities" and only a naked singularity in the very center is possible. The proof uses an assumption that

the SF self-interaction potential is exponentially bounded [46]. Thus, the singularity for any non-zero value of the radial variable in the curvature (Schwarzschild) coordinates is prohibited and the question arises whether this result will be preserved in the case of a sharper dependence of the SF potential for the large field values? This is a key point of the present paper.

In this article, our goal is to provide examples showing that in the case of a sufficiently strong nonlinear behavior of the potential (with a sufficiently fast growth rate), spherical singularities (SS) can arise. To relax the restrictions of [46], we choose $V(\phi) = \sinh(\phi^{2n})$, $n > 2$ as a representative of such potentials. This is a technically convenient choice: for large ϕ, this potential grows faster than any exponentially bounded function; on the other hand, for small ϕ it behaves as a monomial potential that allows us to use earlier results concerning asymptotic behavior $\phi(r) \sim r^{-1}$ for $r \to \infty$.

The paper is organized as follows. In Section 2 we present initial relations. In Sections 3 and 4 we show the possibility of "spherical singularities" and present numerical solutions for the Einstein equations with SF in the case of spherical symmetry. In Section 5 we study distributions of the stable circular orbits (SCO), which is important to study a thin accretion disk around the configuration. We also estimate the radiation flux from the accretion disk within the Page–Thorne model [47].

2. Initial Relations

We consider a static spherically symmetric space-time metric in the curvature coordinates, that is

$$ds^2 = e^{\alpha}dt^2 - e^{\beta}dr^2 - r^2\left[d\theta^2 + \sin^2\theta d\varphi^2\right]; \tag{1}$$

this fixes the radial variable $r > 0$.

The gravitational field interacts with real SF $\phi(r)$ described by Lagrangian density

$$L = \frac{1}{2}\partial_\mu\phi\partial^\mu\phi - V(\phi); \tag{2}$$

the SF potential is

$$V(\phi) = \sinh(\phi^{2n}). \tag{3}$$

This potential is strongly nonlinear for $\phi \to \infty$ and for $n \geq 1$ it grows faster than $|\phi|^a \exp(b\phi)$ for any a, b.

The SF equation following from (2) is

$$\frac{d}{dr}\left[r^2 e^{\frac{\alpha-\beta}{2}}\frac{d\phi}{dr}\right] = r^2 e^{\frac{\alpha+\beta}{2}}V'(\phi) \tag{4}$$

The independent from (4) Einstein equations are reduced to the form (see, e.g., [46])

$$\alpha' + \beta' = 8\pi r\phi'^2, \tag{5}$$

$$\beta' - \alpha' = \frac{2}{r}\left(1 - e^{\beta}\right) + 16\pi r e^{\beta}V(\phi), \tag{6}$$

We focus on isolated systems with mass M in the asymptotically flat space-time assuming for $r \to \infty$

$$\lim_{r\to\infty}[r\alpha(r)] = -\lim_{r\to\infty}[r\beta(r)] = -r_g, \;\; r_g = 2M > 0. \tag{7}$$

As for SF, we assume $\phi(\infty) = 0$; then for (3) we have $V(\phi) \approx \phi^{2n}$ for $r \to \infty$ and therefore we can use some of the results on monomial potentials from [46,48], concerning asymptotic behavior for large r:

$$\phi(r) \sim \exp(-\mu r)/r^{1+\mu M}$$

for $n = 1$ (linear massive scalar field with mass μ [49]);

$$\phi(r) \sim \left\{ \frac{1}{r^{1/(n-1)}},\ 1 < n < 2; \quad \frac{1}{r\sqrt{|\ln r|}},\ n = 2; \quad \frac{1}{r},\ n > 2; \right\} \tag{8}$$

(see Appendix A of [46]); asymptotic relations for $\phi'(r)$ can be obtained by formal differentiation of (8).

3. Asymptotic Behavior Near Singularity

First of all we note that for regular solutions of (4)–(6) within some interval (r_0, ∞), $r_0 > 0$, satisfying conditions (8) with non-trivial $\phi(r)$, we can show that functions $\phi(r)$ and $\phi'(r)$ preserve their signs. Indeed, for potential (3) inequality $\phi V'(\phi) > 0$ is valid for $\phi \neq 0$, and using Equation (4) we get

$$\frac{d}{dr}\left[r^2 e^{\frac{\alpha-\beta}{2}} \phi\, \frac{d\phi}{dr}\right] = r^2 e^{\frac{\alpha+\beta}{2}} \phi\, V'(\phi) + r^2 e^{\frac{\alpha-\beta}{2}} \left[\frac{d\phi}{dr}\right]^2 > 0. \tag{9}$$

Therefore, function $r^2 e^{\frac{\alpha-\beta}{2}} \phi\, \phi'$ is monotonically increasing. On account of conditions (7) and (8), it is strictly negative for large r; therefore it cannot be equal to zero and so is $\phi(r)\phi'(r) < 0$. Whence we infer that functions $\phi(r)$, $\phi'(r)$ do not change their signs.

Further, for definiteness, we assume $\phi(r) > 0$, $\phi'(r) < 0$.

Now we turn to the singularities at some $r_s > 0$ in case of potential (3). We are looking for solutions on (r_s, ∞) such that

$$\phi'(r) \to -\infty,\ r \to r_s + 0, \tag{10}$$

for some $r_s > 0$. Our aim is to estimate asymptotic properties of these solutions.

Equations (5) and (6) yield

$$\beta' = 4\pi r \phi'^2 + \frac{1}{r}\left(1 - e^{\beta}\right) + 8\pi r e^{\beta} V(\phi). \tag{11}$$

Numerical simulations near singularity suggests that $\alpha(r)$ is a slowly varying function. So, as a first approximation, we are neglecting this function compared to $\beta(r)$. Under this assumption we get for the leading terms of Equation (4)

$$e^{-\beta/2} \frac{d}{dr}\left[e^{-\beta/2}\phi'\right] \simeq V'(\phi). \tag{12}$$

This is a rough approximation that is valid in very small interval near the singularity. We have then $e^{-\beta}\phi'^2 \simeq 2V(\phi) + const$, where the constant will be neglected in comparison with $V(\phi)$ for $r \to r_s + 0$, so that

$$e^{-\beta}\phi'^2 \simeq 2V(\phi). \tag{13}$$

In view of (10), $e^{\beta}V(\phi) \simeq \phi'^2 \to \infty$ for $r \to r_s + 0$ and then it is easy to see that the principal terms on the right hand sides of (5) and (6) are asymptotically the same. This justifies our assumption about $\alpha(r)$.

Substitution into (11) yields

$$\beta' \simeq 16\pi r e^{\beta} V(\phi), \tag{14}$$

where we discarded the lower order terms. This allows us to reduce the problem to the system of two equations.

Then $\beta(r)$ is monotonically increasing (for $r \in (r_s, r_1]$, where $(r_1 - r_s)/r_s \ll 1$). For $r \to r_s + 0$ Equation (14) yields

$$\frac{d}{dr}\left[e^{-\beta/2}\right] \approx -8\pi r_s e^{\beta/2} V(\phi). \tag{15}$$

From Equation (13) we have

$$\phi' \approx -\sqrt{2} e^{\beta/2} \sqrt{V(\phi)}, \tag{16}$$

where we take into account that $\phi(r)$ is decreasing.

Dividing (15) by (16) we have equation

$$\frac{d}{d\phi}\left[e^{-\beta/2}\right] = \frac{8\pi r_s}{\sqrt{2}} \sqrt{V(\phi)}$$

that can be solved in quadratures. In the leading terms for $r \to r_s + 0$

$$e^{-\beta(r)/2} \simeq \frac{8\pi r_s}{\sqrt{2}} \Phi(\phi) + e^{-\beta(r_1)/2} \sim \frac{8\pi r_s}{\sqrt{2}} \Phi(\phi) \tag{17}$$

where we denote

$$\Phi(\phi) = \int_{\phi(r_1)}^{\phi} \sqrt{V(x)} dx = \int_{\phi(r_1)}^{\phi} \exp\left(\frac{1}{2} x^{2n}\right) dx.$$

This can be expressed by the incomplete gamma-function, leading to the asymptotic formula:

$$\Phi(\phi) = \frac{1}{n\phi^{2n-1}} \sqrt{V(\phi)} \left[1 + O\left(\frac{1}{\phi}\right)\right], \; r \to r_s. \tag{18}$$

Then we use (17), (18) to get from (16)

$$\frac{d\phi}{dr} = -\frac{\sqrt{V(\phi)}}{4\pi r_s \Phi(\phi)} \simeq -\frac{n}{4\pi r_s} \phi^{2n-1}.$$

The solution is

$$\phi(r) = \left\{ \frac{n(n-1)}{2\pi} \frac{r - r_1}{r_s} + \frac{1}{\phi_1^{2(n-1)}} \right\}^{-\frac{1}{2(n-1)}}, \quad \phi_1 = \phi(r_1).$$

The limit (10) occurs if

$$\frac{n(n-1)}{2\pi} \cdot \frac{r_1 - r_s}{r_s} = \frac{1}{\phi_1^{2(n-1)}} \tag{19}$$

Then

$$\phi(r) \sim \left\{ \frac{2\pi r_s}{n(n-1)(r - r_s)} \right\}^{\frac{1}{2(n-1)}}. \tag{20}$$

Using (17) we have

$$\beta(r) \sim -2 \ln \Phi(\phi) \sim -\left[\frac{2\pi r_s}{n(n-1)(r - r_s)} \right]^{n/(n-1)}. \tag{21}$$

The Kretschmann invariant near r_s has the form

$$R_{\alpha\beta\gamma\delta}R^{\alpha\beta\gamma\delta} \sim \frac{e^{-2\beta(r)}}{(r-r_s)^{\frac{2(2n-1)}{n-1}}}. \tag{22}$$

The main outcome of these considerations is that there exist singularities of solutions to systems (4)–(6) for some non-zero value of the radial variable in curvature coordinates, that is, SS are indeed possible. This does not mean that all the solutions have such singularities. It easy to see that for $n > 1$ to have the singularity at some $r = r_s > 0$, the condition (19) must be fulfilled (i.e., ϕ_1 must be sufficiently large). The latter depends on the initial conditions at infinity and this must be derived numerically. This is a subject of the next section.

4. Numerical Solutions

Here we restrict ourselves to the case of a long-range field $n > 2$. Correspondingly, taking into account (8), we assume the conditions for the field

$$\lim_{r\to\infty}\left[r^2\frac{d\phi}{dr}\right] = -Q \tag{23}$$

yielding

$$\lim_{r\to\infty}[r\phi(r)] = Q. \tag{24}$$

It was shown in [48] that there is a unique solution of the problem for sufficiently large r satisfying (4)–(6) and (24). The iteration procedure yielding the solution is described in [48] for a monomial potential and it can be applied in case of (3) for sufficiently large r (small ϕ). This yields initial conditions for the ordinary differential system (4)–(6) at some (large) r_{init}. Instead, one can directly use asymptotic expansions to derive the solution for large r_{init}. We obtained the solution numerically by integrating the equations backward from r_{init} to smaller values of r, either to a spherical singularity or to a point-like naked singularity at the origin. The occurrence of singularity can be checked by means of relation (19); this can be used in order to define more precisely the singularity radius.

Figures 1 and 2 show typical behavior of solutions in the case of SS; we see that e^α is monotonically increasing, whereas e^β reaches a maximum and then decreases to one for $r \to \infty$. Additionally, we note that near the singularity $e^{\beta-\alpha} \to 0$ for $r \to r_s + 0$ in accordance with Section 3. Figures 3–5 show a non-trivial dependence of the singularity radii r_s upon parameters n, M, Q.

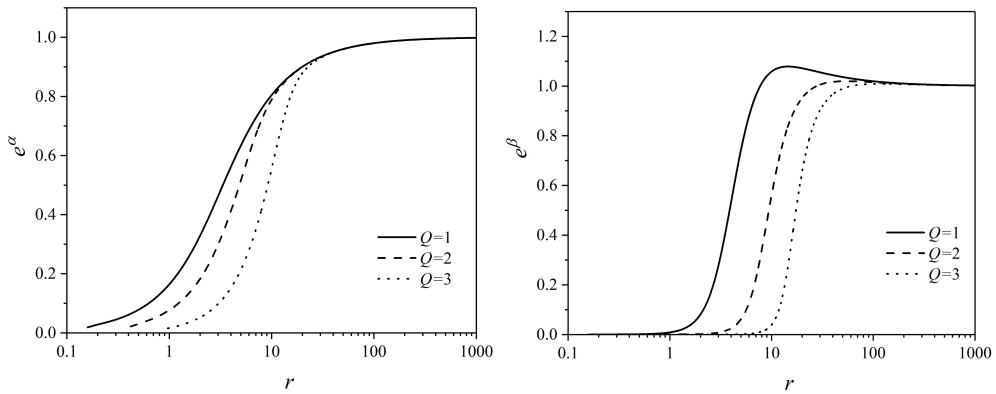

Figure 1. Behavior of metric functions e^α (**left**) and e^β (**right**) for $M = 1$ and different Q.

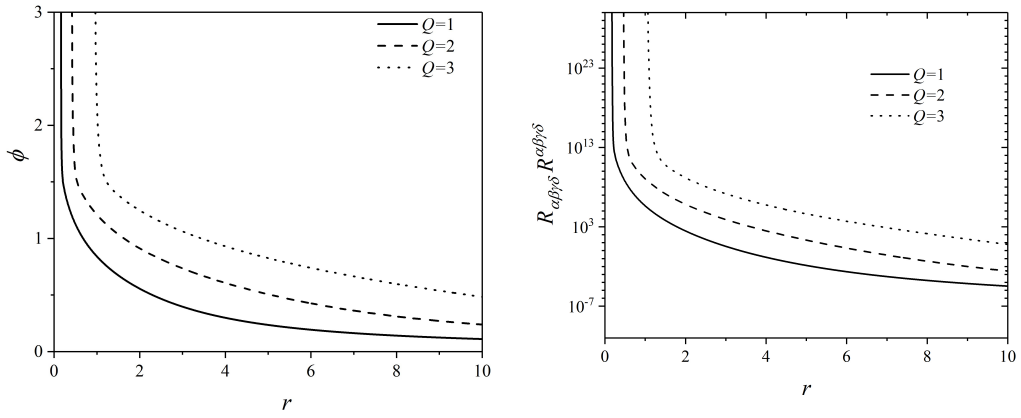

Figure 2. Behavior of SF (**left**) and Kretschmann invariant $R_{\alpha\beta\gamma\delta}R^{\alpha\beta\gamma\delta}$ (**right**) for the same parameters.

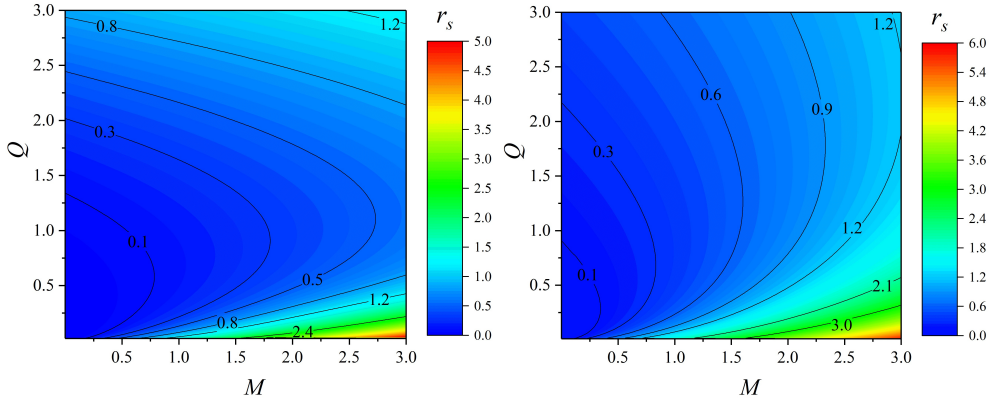

Figure 3. Radii of SS for different M, Q; $n = 6$ (**left**), $n = 18$ (**right**).

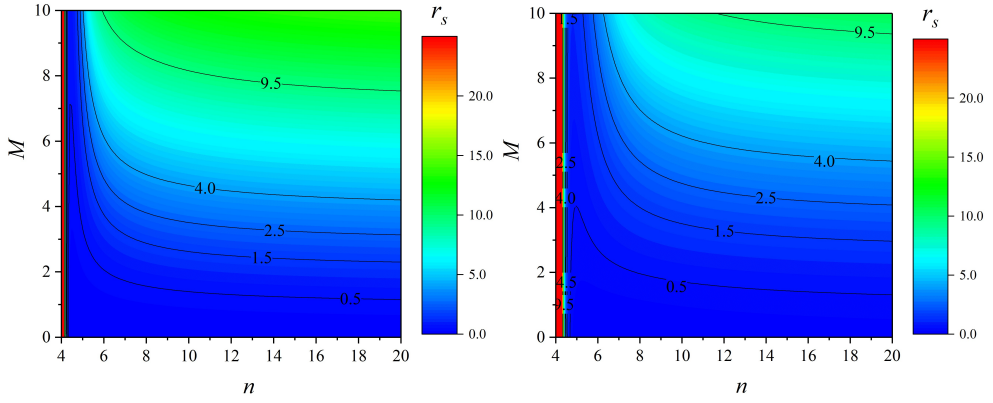

Figure 4. Radii of SS for different n, M; $Q = 0.5$ (**left**), $Q = 1$ (**right**).

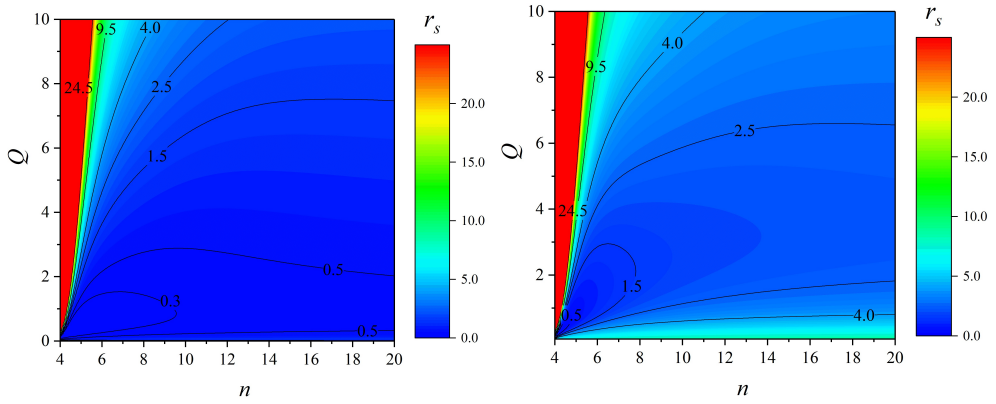

Figure 5. Radii of SS for different n, Q; $M = 1$ (**left**) and $M = 5$ (**right**).

5. Test Particle Motion

In this section, we consider the massive test particles motion around static spherically symmetric configurations with SF to describe in order to describe characteristics of accretion onto a singularity. We use the Page–Thorne model [47] of a thin accretion disk (AD). In this model, the averaged motion of the accreting matter is essentially described by SCOD in the equatorial plane.

In the case of spherically symmetric space-time with metric (1), the standard procedure yields the first integrals for test particle trajectories in the equatorial plane $\theta = \pi/2$ (τ is a canonical parameter.):

$$e^{\alpha}\left(\frac{dt}{d\tau}\right)^2 - e^{\beta}\left(\frac{dr}{d\tau}\right)^2 - r^2\left(\frac{d\phi}{d\tau}\right)^2 = S\,, \tag{25}$$

$$e^{\alpha}\left(\frac{dt}{d\tau}\right) = E, \quad r^2\left(\frac{d\phi}{d\tau}\right) = L\,, \tag{26}$$

where $S = 0$ in case of null trajectories and $S = 1$ for the test particles with the non-zero mass; L, E are the integrals of motion. This yields

$$e^{\alpha+\beta}\left(\frac{dr}{d\tau}\right)^2 = E^2 - U_{\rm eff}(r, L, S)\,, \tag{27}$$

where effective potential $U_{\rm eff}(r, L, S) = e^{\alpha}\left(S + L^2/r^2\right)$.

The form of $U_{\rm eff}(r)$, in particular, the disposition of its minima and maxima, defines the distribution of stable circular orbits (SCO) and unstable ones. The SCO distribution (SCOD) is the most important because it forms the basis for evaluating the properties of an accretion disc around the configuration described by Equations (4)–(6). Possible types of SCODs are listed in Table 1 and described schematically on Figure 6.

Table 1. Possible types of SCOD.

Type	$r_{\rm stable}$	$r_{\rm unstable}$	Photon Sphere
$U_1^{(-)}$	(r_1, ∞)	(r_s, r_1)	−
$U_1^{(+)}$	(r_1, ∞)	(r_s, r_1)	+
U_2	$(r_1, r_2) \cup (r_3, \infty)$	$(r_s, r_1) \cup (r_2, r_3)$	−

We use a method of our works [13,49] to study bifurcations associated with the appearance and disappearance of the minima of $U_{\rm eff}$. Figure 7 illustrates how the shape of the effective potential changes with an increase in L in case of the U_2 SCOD type. Essentially

this is connected with investigation of joint conditions $U'_{\rm eff} = 0$ and $U''_{\rm eff} = 0$, which allow us to exclude L; this leads to a necessary condition $F(r) = 0$, where

$$F(r) = r\alpha''(r) - r\alpha'(r)^2 + 3\alpha'(r). \tag{28}$$

For the congruence of circular orbits with different radii in equatorial plane we get dependencies of the specific energy and the specific angular momentum, and the angular velocity $\Omega = d\varphi/dt$ upon radius r as follows

$$\tilde{E}^2(r) = \frac{2e^{\alpha(r)}}{2 - r\alpha'(r)}, \quad \tilde{L}^2(r) = \frac{r^3\alpha'(r)}{2 - r\alpha'(r)}, \quad \Omega^2(r) = \frac{\alpha'(r)e^{\alpha(r)}}{2r} \tag{29}$$

Using Equation (28), we numerically get the bifurcation values r_b, $L_b^2 = \tilde{L}^2(r_b)$ and $E_b^2 = \tilde{E}^2(r_b)$ under conditions that $\tilde{E}^2(r_b) > 0$ and $\tilde{L}^2(r_b) > 0$. This allows us to determine SCOD types for given configuration parameters. Figure 8 shows the corresponding results in the $M - Q$ plane. Also, Figure 9 illustrates the dependence of the boundary radii (i.e., radii of the blue circles in Figure 6) upon M and Q.

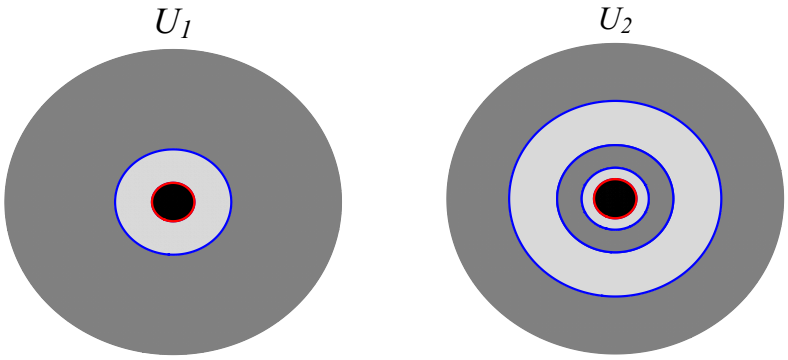

Figure 6. The schematic examples of possible SCODs in the equatorial plane. In both cases, black spots in the center represent SS at finite values of r. Dark and light gray rings correspond to the sequences of SCO and unstable circular orbits correspondingly. Blue circles show the boundary radii of SCOD as described in Table 1.

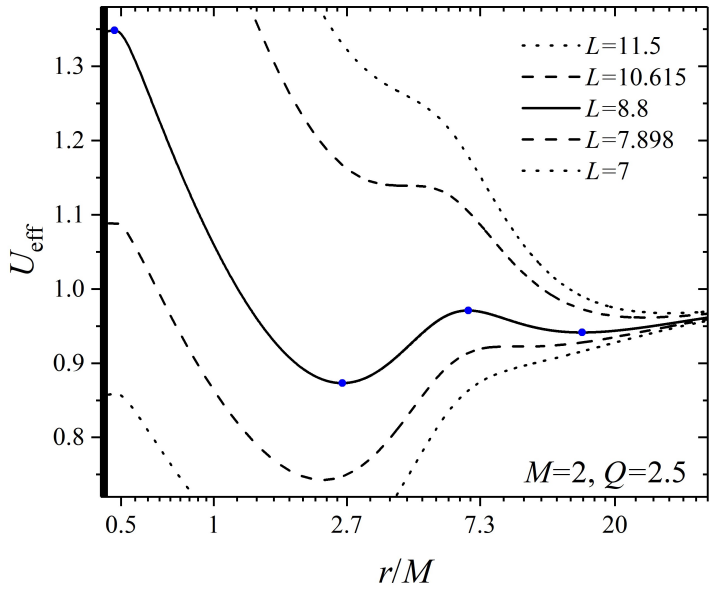

Figure 7. Typical examples of $U_{\rm eff}$ for configuration with U_2 SCOD type. The blue points show the corresponding extrema. There is only one minimum for large L.

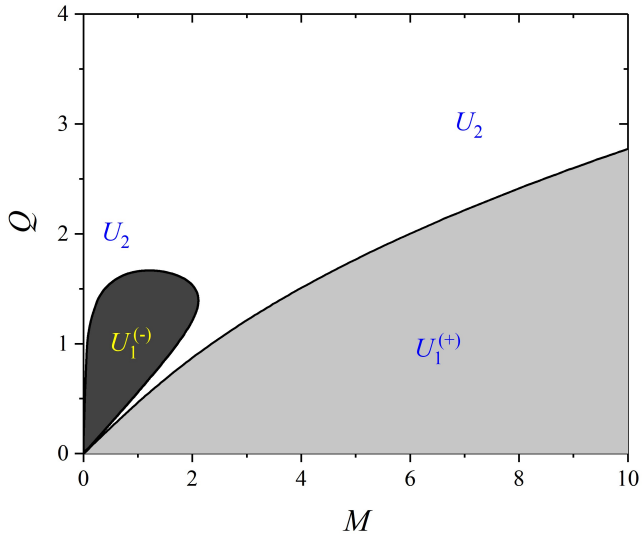

Figure 8. Domains of parameters on (M, Q) plane for $n = 3$. Every point of this plane corresponds to a solution of Equations (4)–(6) with conditions (7), (8). The SCOD type was determined for every such solution; gray, dark gray and white colors correspond to the $U_1^{(+)}$, $U_1^{(-)}$ and U_2 type, respectively.

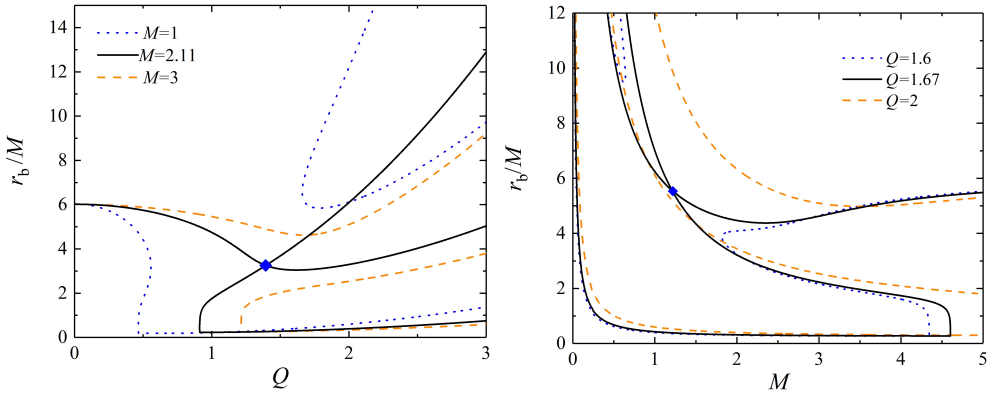

Figure 9. Boundary radii r_b/M of SCO regions as functions of Q (**left**) and M (**right**) for several values of M and Q. The corresponding points where curves qualitatively change their behavior by reconnection are $(M, Q) \simeq (2.11, 1.39)$ and $(M, Q) \simeq (1.2, 1.67)$ for left and right pictures, respectively and shown by blue squares.

Now we consider radiation from the stationary thin AD described by Page–Thorne model [47]. The time averaged radiation flux $F(r)$ from the surface of the accretion with inner edge located at the boundary SCO $r = r_{\rm b}$ is

$$F(r) = -\frac{\dot{M}_0}{4\pi\sqrt{|^{(3)}g|}}\frac{\Omega_{,r}}{(E-\Omega L)^2}\int_{r_{\rm b}}^{r}(E-\Omega L)L_{,x}\,dx, \tag{30}$$

where $\sqrt{|^{(3)}g|} = re^{(\alpha+\beta)/2}$ is the metric's determinant in the equatorial plane and $\dot{M}_0$ is the mass accretion rate that is assumed to be constant. Specific particle energy, momentum, and angular velocity are defined from (29). We obtained the radiation flux for several values Q in presence/absence of inner stable ring of AD. The corresponding fluxes are shown in Figure 10. To compare different types, we normalize them to the maximum flux in the case of a Schwarzschild black hole $F_{\rm Schw}^{(\max)} \simeq 0.0001719\dot{M}_0/4\pi M^2$. We see that the maximum value of different types can be less or more then 1 as distinct from the case of the massless scalar field [29,33], where $F/F_{\rm Schw}^{(\max)} \geq 1$ due to $r_b \leq 6M$.

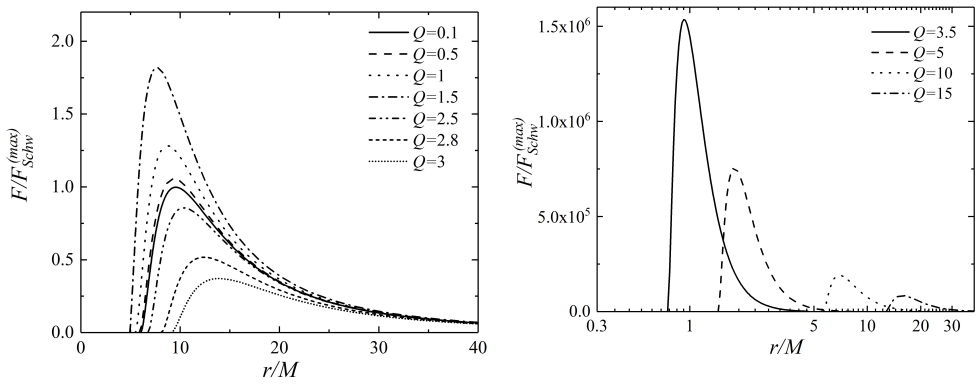

Figure 10. The normalized flux ($M = 4$) from inner (**right**) and outer (**left**) parts of AD.

6. Discussion

We have shown that General Relativity allows the existence of SS in static spherically symmetric configurations in the case of the SF potential $V(\phi) = \sinh(\phi^{2n})$, which represents potentials with fast growth rate. This statement follows from the analytical reasoning of Section 3 and is confirmed by numerical simulations of Section 4. These SS are "physical" singularities that cannot be removed by a coordinate transformation: this can be seen from the behavior of the Kretschmann invariant. These are naked singularities, because they can be observed by a distant observer; it is easy to verify this by considering the radial motion of photons, taking into account that near the singularity $\exp(\beta - \alpha) \to 0$ for $r \to r_s + 0$.

We note that the appearance of singularities in solutions of nonlinear equations is a fairly typical case. However, the situation with SS is different from the case of monomial or the other exponentially bounded potentials, when SS are suppressed by the gravitational field and we only have a naked singularity at the center [46]. In the case of $V(\phi) = \sinh(\phi^{2n})$, the sharp growth of the field near the singularity overcomes this suppression. This suggests that SS can occur for more general potentials with fairly rapid growth.

Having the numerical solutions, we investigated the location of stable and unstable circular orbits. There are two main types of SCOD in our case: (i) U_1 is similar to SCOD in the case of the Schwarzschild metric, when SCO radii must be larger than some boundary value; (ii) U_2 type is formed by a non-connected distribution with two regions of SCO separated by a ring of unstable circular orbits. These distributions of the stable orbits are directly related to the structure of the thin accretion disk in the Page–Thorne model [47]. Perhaps this result can also be important for more complex AD models, if, of course, the above scalar fields do exist. Note that these types of SCODs also arise in the case of solutions with monomial potentials [48]. Additionally, it should be noted that U_2 type is not observed for M87* shadow [28]. However, for definite answer observations with better resolution are mandatory.

We have no answer to the question of whether strongly nonlinear fields really exist. Moreover, the question remains, how the spherical singularity can form. This is a question of the same order as the origin of point naked singularities, as well as other exotic structures such as bosonic stars, wormholes, etc. [4–13,15–26]. We note, however, that for some sets of configuration parameters, it could be difficult to distinguish SS from ordinary black holes relying upon the accretion disk structures. On the other hand, for other sets of parameters, we may have an unconnected SCO region, which would be different from the point of view of a distant observer. Additional information on the existence/non-existence of the strongly non-linear scalar fields may come from considerations of early cosmological processes. So the hypothesis of the existence of the spherical singularities seems to be testable.

Author Contributions: O.S.: Conceptualization, writing—original draft. V.I.Z.: Conceptualization, writing—original draft, supervision. All authors have read and agreed to the published version of the manuscript.

Funding: Funded by the National Research Foundation of Ukraine (project No. 2020.02/0073).

Acknowledgments: We are grateful to the anonymous referee for helpful comments.

Conflicts of Interest: The authors declare no conflict of interest.

References

1. Novikov, I.D.; Thorne, K.S. Astrophysics of black holes. In *Black Holes (Les Astres Occlus)*; DeWitt, C., DeWitt, B., Eds.; Gordon and Breach: New York, NY, USA, 1973; pp. 343–450.
2. Antonucci, R. Unified Models for Active Galactic Nuclei and Quasars. *Annu. Rev. Astron. Astrophys.* **1993**, *31*, 473–521. [CrossRef]
3. Bianchi, S.; Maiolino, R.; Risaliti, G. AGN Obscuration and the Unified Model. *Adv. Astron.* **2012**, *2012*, 782030. [CrossRef]
4. Stuchlík, Z.; Schee, J. Optical effects related to Keplerian discs orbiting Kehagias-Sfetsos naked singularities. *Class. Quantum Gravity* **2014**, *31*, 195013. [CrossRef]
5. Shao, W.H.; Chen, C.Y.; Chen, P. Generating rotating spacetime in Ricci-based gravity: Naked singularity as a black hole mimicker. *J. Cosmol. Astropart. Phys.* **2021**, *2021*, 041. [CrossRef]
6. Chakraborty, C.; Bhattacharyya, S. Circular orbits in Kerr-Taub-NUT spacetime and their implications for accreting black holes and naked singularities. *J. Cosmol. Astropart. Phys.* **2019**, *2019*, 034. [CrossRef]
7. Bhattacharya, K.; Dey, D.; Mazumdar, A.; Sarkar, T. New class of naked singularities and their observational signatures. *Phys. Rev. D* **2020**, *101*, 043005. [CrossRef]
8. Pugliese, D.; Quevedo, H.; Ruffini, R. Circular motion of neutral test particles in Reissner-Nordström spacetime. *Phys. Rev. D* **2011**, *83*, 024021. [CrossRef]
9. Pugliese, D.; Quevedo, H.; Ruffini, R. Equatorial circular orbits of neutral test particles in the Kerr-Newman spacetime. *Phys. Rev. D* **2013**, *88*, 024042. [CrossRef]
10. Joshi, P.S.; Malafarina, D.; Narayan, R. Distinguishing black holes from naked singularities through their accretion disc properties. *Class. Quantum Gravity* **2013**, *31*, 015002. [CrossRef]
11. Shahidi, S.; Harko, T.; Kovács, Z. Distinguishing Brans–Dicke–Kerr type naked singularities and black holes with their thin disk electromagnetic radiation properties. *Eur. Phys. J. C* **2020**, *80*, 1–20. [CrossRef]
12. Boshkayev, K.; Gasperín, E.; Gutiérrez-Piñeres, A.C.; Quevedo, H.; Toktarbay, S. Motion of test particles in the field of a naked singularity. *Phys. Rev. D* **2016**, *93*, 024024. [CrossRef]
13. Stashko, O.S.; Zhdanov, V.I. Spherically symmetric configurations of General Relativity in presence of scalar fields: Separation of circular orbits. *Gen. Relativ. Gravit.* **2018**, *50*, 105. [CrossRef]
14. Bambhaniya, P.; Joshi, A.B.; Dey, D.; Joshi, P.S. Timelike geodesics in naked singularity and black hole spacetimes. *Phys. Rev. D* **2019**, *100*, 124020. [CrossRef]
15. Karimov, R.K.; Izmailov, R.N.; Nandi, K.K. Accretion disk around the rotating Damour–Solodukhin wormhole. *Eur. Phys. J. C* **2019**, *79*, 1–9. [CrossRef]
16. Paul, S.; Shaikh, R.; Banerjee, P.; Sarkar, T. Observational Signatures of Wormholes with Thin Accretion Disks. *J. Cosmol. Astropart. Phys.* **2020**, *3*, 055. [CrossRef]
17. Narzilloev, B.; Malafarina, D.; Abdujabbarov, A.; Ahmedo, B.; Bambi, C. Particle Motion around a Static Axially Symmetric Wormhole. *Phys. Rev. D* **2021**, *104*, 064016. [CrossRef]
18. Abdujabbarov, A.A.; Ahmedov, B.J. Electromagnetic fields and charged particle motion around magnetized wormholes. *Astrophys. Space Sci.* **2009**, *321*, 225–232. [CrossRef]
19. Li, Z.; Bambi, C. Distinguishing black holes and wormholes with orbiting hot spots. *Phys. Rev. D* **2014**, *90*, 024071. [CrossRef]
20. Vincent, F.H.; Meliani, Z.; Grandclément, P.; Gourgoulhon, E.; Straub, O. Imaging a boson star at the Galactic center. *Class. Quantum Gravity* **2016**, *33*, 105015. [CrossRef]
21. Grandclément, P.; Somé, C.; Gourgoulhon, E. Models of rotating boson stars and geodesics around them: New type of orbits. *Phys. Rev. D* **2014**, *90*. [CrossRef]
22. Liebling, S.L.; Palenzuela, C. Dynamical boson stars. *Living Rev. Relativ.* **2017**, *20*, 5. [CrossRef]
23. Lamy, F.; Gourgoulhon, E.; Paumard, T.; Vincent, F.H. Imaging a non-singular rotating black hole at the center of the Galaxy. *Class. Quantum Gravity* **2018**, *35*, 115009. [CrossRef]
24. Herdeiro, C.A.; Pombo, A.M.; Radu, E.; Cunha, P.V.; Sanchis-Gual, N. The imitation game: Proca stars that can mimic the Schwarzschild shadow. *J. Cosmol. Astropart. Phys.* **2021**, *2021*, 051. [CrossRef]
25. Dymnikova, I.; Poszwa, A. Classification and basic properties of circular orbits around regular black holes and solitons with the de Sitter center. *Class. Quantum Gravity* **2019**, *36*, 105002. [CrossRef]
26. Stuchlík, Z.; Schee, J. Circular geodesic of Bardeen and Ayon–Beato–Garcia regular black-hole and no-horizon spacetimes. *Int. J. Mod. Phys. D* **2015**, *24*, 1550020. [CrossRef]

27. Schönenbach, T.; Caspar, G.; Hess, P.O.; Boller, T.; Müller, A.; Schäfer, M.; Greiner, W. Ray-tracing in pseudo-complex General Relativity. *Mon. Not. R. Astron. Soc.* **2014**, *442*, 121–130. [CrossRef]
28. Event Horizon Telescope Collaboration. First M87 Event Horizon Telescope Results. I. The Shadow of the Supermassive Black Hole. *Astrophys. J.* **2019**, *875*, L1. [CrossRef]
29. Chowdhury, A.N.; Patil, M.; Malafarina, D.; Joshi, P.S. Circular geodesics and accretion disks in the Janis-Newman-Winicour and gamma metric spacetimes. *Phys. Rev. D* **2012**, *85*, 104031. [CrossRef]
30. Zhou, S.; Zhang, R.; Chen, J.; Wang, Y. Geodesic Structure of Janis-Newman-Winicour Space-time. *Int. J. Theor. Phys.* **2015**, *54*, 2905–2920. [CrossRef]
31. Shaikh, R.; Joshi, P.S. Can we distinguish black holes from naked singularities by the images of their accretion disks? *J. Cosmol. Astropart. Phys.* **2019**, *2019*, 064. [CrossRef]
32. Gyulchev, G.; Nedkova, P.; Vetsov, T.; Yazadjiev, S. Image of the Janis-Newman-Winicour naked singularity with a thin accretion disk. *Phys. Rev. D* **2019**, *100*, 024055. [CrossRef]
33. Gyulchev, G.; Kunz, J.; Nedkova, P.; Vetsov, T.; Yazadjiev, S. Observational signatures of strongly naked singularities: Image of the thin accretion disk. *Eur. Phys. J. C* **2020**, *80*, 1–20. [CrossRef]
34. Gyulchev, G.; Nedkova, P.; Vetsov, T.; Yazadjiev, S. Image of the thin accretion disk around compact objects in the Einstein-Gauss-Bonnet gravity. *arXiv* **2021**, arXiv:2106.14697.
35. Collodel, L.G.; Doneva, D.D.; Yazadjiev, S.S. Circular Orbit Structure and Thin Accretion Disks around Kerr Black Holes with Scalar Hair. *Astrophys. J.* **2021**, *910*, 52. [CrossRef]
36. Sau, S.; Banerjee, I.; SenGupta, S. Imprints of the Janis-Newman-Winicour spacetime on observations related to shadow and accretion. *Phys. Rev. D* **2020**, *102*, 064027. [CrossRef]
37. Cao, Z.; Cárdenas-Avendaño, A.; Zhou, M.; Bambi, C.; Herdeiro, C.A.; Radu, E. Iron Kα line of boson stars. *J. Cosmol. Astropart. Phys.* **2016**, *2016*, 003. [CrossRef]
38. Yang, J.; Ayzenberg, D.; Bambi, C. Iron line spectroscopy of black holes in vector-tensor Galileon modified gravity. *Phys. Rev. D* **2018**, *98*, 044024. [CrossRef]
39. Shen, T.; Zhou, M.; Bambi, C.; Herdeiro, C.A.R.; Radu, E. Iron Kα line of Proca stars. *J. Cosmol. Astropart. Phys.* **2017**, *2017*, 014. [CrossRef]
40. Liu, H.; Zhou, M.; Bambi, C. Distinguishing black holes and naked singularities with iron line spectroscopy. *J. Cosmol. Astropart. Phys.* **2018**, *2018*, 044. [CrossRef]
41. Martínez, C.; Troncoso, R.; Zanelli, J. Exact black hole solution with a minimally coupled scalar field. *Phys. Rev. D* **2004**, *70*. [CrossRef]
42. Fisher, I.Z. Scalar mesostatic field with regard for gravitational effects. *Zh. Exp. Theor. Phys.* **1948**, *18*, 636–640.
43. Janis, A.I.; Newman, E.T.; Winicour, J. Reality of the Schwarzschild Singularity. *Phys. Rev. Lett.* **1968**, *20*, 878–880. [CrossRef]
44. Wyman, M. Static spherically symmetric scalar fields in general relativity. *Phys. Rev. D* **1981**, *24*, 839–841. [CrossRef]
45. Virbhadra, K.S. Janis–Newman–Winicour and Wyman Solutions are the Same. *Int. J. Mod. Phys. A* **1997**, *12*, 4831–4835. [CrossRef]
46. Zhdanov, V.I.; Stashko, O.S. Static spherically symmetric configurations with N nonlinear scalar fields: Global and asymptotic properties. *Phys. Rev. D* **2020**, *101*, 064064. [CrossRef]
47. Page, D.N.; Thorne, K.S. Disk-Accretion onto a Black Hole. Time-Averaged Structure of Accretion Disk. *Astrophys. J.* **1974**, *191*, 499–506. [CrossRef]
48. Stashko, O.S.; Zhdanov, V.I.; Alexandrov, A.N. Thin Accretion Discs around Spherically Symmetric Configurations with Nonlinear Scalar Fields. *arXiv* **2021**, arXiv:2107.05111.
49. Stashko, O.; Zhdanov, V. Spherically Symmetric Configurations in General Relativity in the Presence of a Linear Massive Scalar Field: Separation of a Distribution of Test Body Circular Orbits. *Ukr. J. Phys.* **2019**, *64*, 189. [CrossRef]